Behavioral/Cognitive

Hemifield Specificity of Attention Response Functions during Multiple-Object Tracking

Marvin R. Maechler,[1] Eunhye Choe,[1] Patrick Cavanagh,[2] Peter J. Kohler,[3] and Peter U. Tse[1]

[1]Department of Psychological and Brain Sciences, Dartmouth College, Hanover, New Hampshire 03755, [2]Department of Psychology, Glendon College, Toronto, Ontario M4N 3M6, Canada, and [3]Department of Psychology, York University, Toronto, Ontario L4K 4N5, Canada

The difficulty of tracking multiple moving objects among identical distractors increases with the number of tracked targets. Previous research has shown that the number of targets tracked (i.e., load) modulates activity in brain areas related to visuospatial attention, giving rise to so-called attention response functions (ARFs). While the hemifield/hemispheric effects of spatial attention (e.g., hemispatial neglect, hemifield capacity limits) are well described, it had not previously been tested whether a hemispheric or hemifield imbalance exists among ARFs. By recording blood oxygenation level-dependent activity from human brains ($n = 19$, female and male) in a multiple-object tracking paradigm, we show that the number of tracked objects modulates activity in a large network of areas bilaterally. A significant effect of contralateral load was found in earlier areas throughout the dorsal and ventral visual streams, while the effects of ipsilateral load emerged in later areas. Both contra- and ipsilateral load significantly influenced activity in the parietal and frontal lobes, specifically the dorsal attention network. In addition, some brain regions in the occipital lobe were significantly more sensitive to contralateral than ipsilateral load. Our results are consistent with findings showing that a diverse set of brain areas contributes to tracking multiple targets. In particular, we extend the canonical view of load-based ARFs to include hemifield bias. Given the hemifield-specific nature of speed and capacity limits to multiple-object tracking, we conjecture that areas that show a strong hemifield preference may impose a bottleneck on processing that results in limits on the capacity and speed of tracking.

Key words: attention; attentional tracking; hemisphere specificity; mental effort; multiple-object tracking

---

Significance Statement

We investigated how attentional effort impacts brain activity. Effort (the number of targets in a multiple-object tracking task) parametrically drives activity in the attention system. Our findings reveal brain areas where effort-driven increases in activity are dependent on the visual hemifield where targets are tracked. We show that the load-dependent responses differ between earlier visual areas, which prefer targets on the contralateral side, and later areas that respond to targets anywhere in the visual field. This research challenges previous explanations of hemispatial neglect and enhances our understanding of how the brain manages spatial attention and mental effort. Additionally, we identify regions that might be the source of hemifield-specific capacity limits in attentional tracking.

Introduction

Object tracking is a fundamental function of the visual system. Driving in traffic would be unimaginable without the ability to keep track of target objects as they move. Performance in object tracking tasks is governed by several factors that severely constrain its effectiveness. For example, as objects get closer together or increase in speed, the ability to track them decreases (Intriligator and Cavanagh, 2001; Cavanagh and Alvarez, 2005; Störmer et al., 2014; Maechler et al., 2021; Holcombe, 2023). Additionally, tracking performance drops as the number of tracked targets increases (Alvarez and Cavanagh, 2005; Franconeri et al., 2008; Scholl, 2009).

How does the brain track multiple objects at once? Previous neuroimaging studies have identified several brain areas that may contribute to this task, which broadly fit into two categories. One set of areas show increasing blood oxygenation level-dependent (BOLD) responses as the number of tracked objects increases (i.e., tracking load). In contrast, a second set is comprised of areas that respond during attentional tracking, but their activity is independent of the number of targets tracked. The two kinds of

attention response functions (ARFs) are called load-dependent and task-dependent, respectively (Culham et al., 2001; Jovicich et al., 2001; Shim et al., 2010; Jahn et al., 2012; Alnæs et al., 2014; Nummenmaa et al., 2017). ARFs are typically found in the superior parietal lobule (SPL), the intraparietal sulcus (IPS), and the frontal eye fields (FEF)—all areas that are canonically associated with visuospatial attention. However, they are also found in areas earlier in the visual processing stream such as V3 and hMT.

While these prior studies have provided a great deal of insight into the neural substrate of multiple-object tracking, the underlying mechanism is still debated. For example, although it is well known that some resources for attentional tracking are hemisphere specific (Holcombe and Chen, 2012; Störmer et al., 2014), most of the fMRI studies of ARFs combined results for tracked targets that were contra- or ipsilateral to the brain areas being imaged. This contralateral versus ipsilateral relation is critical, however, because more targets (Alvarez and Cavanagh, 2005) can be successfully tracked at higher speed (Holcombe and Chen, 2012; Störmer et al., 2014) when the targets are distributed across both visual hemifields rather than constrained to just one. Additionally, tracking performance decreases when two targets cross the vertical meridian simultaneously (Strong and Alvarez, 2020). Thus, there is considerable evidence from behavioral studies that tracking processes are to some extent independent within each hemifield. However, this evidence has not previously been considered when investigating ARFs. The present study aims to remedy this lack.

In particular, we ask: Are load-dependent ARFs hemifield specific? In one fMRI study (Shim et al., 2010), ARFs for different brain areas were assessed with respect to whether the targets were contra- or ipsilateral to the brain area. Their results suggested that contra- as well as ipsilateral increases in tracking load increase BOLD activity in the parietal lobe, with ipsilateral targets having a slightly smaller effect. However, in their experiment, the number of targets was only varied from one to two targets, while their speed was manipulated separately. Additionally, Shim et al. (2010) did not observe hemispheric differences and therefore combined regions of interest (ROIs) from the two hemispheres to increase their statistical power.

There is extensive evidence for hemispheric differences in attention, with the right hemisphere being more important for spatial attention. Hemispatial neglect, a neuropsychiatric disorder that renders some stroke survivors unable to attend to the contralesional side of space, occurs predominantly after injuries to the right hemisphere (Parton et al., 2004; Corbetta and Shulman, 2011). The right hemisphere dominance for neglect implies a corresponding asymmetry of the neural circuits underlying spatial attention in healthy brains. Earlier accounts of hemispatial neglect (Mesulam, 1981) claimed that the right hemisphere can deploy spatial attention to both hemifields, while the left hemisphere only does so to its contralateral hemifield. Based on this, one would predict that ARFs in the left hemisphere should show a contralateral bias, while such a bias should be absent or at least weaker in the right hemisphere. More modern explanations of neglect predict a contralateral bias in both hemispheres (Corbetta and Shulman, 2011). In addition to neglect, other hemifield-specific effects of attention have been reported in the literature. For example, spatial attention to the left hemifield is more impacted by high concurrent working memory load than attention to the right hemifield (Naert et al., 2018). Leftward attentional biases are more common among young children, and they decrease during development (Hoyos et al., 2021).

Here we examined the hemifield specificity of load-dependent ARFs. Specifically, we asked whether any brain areas with load-dependent ARFs demonstrate a contralateral bias. To do so, we limited each target's motion to either the left or right hemifield and varied the number of targets in each hemifield independently. We recorded fMRI data while participants tracked between zero and four targets, out of a total of eight objects distributed evenly across both hemifields. The number of targets in each hemifield varied independently between zero and two targets, allowing us to estimate the effect of increasing tracking load in each hemifield.

We found ARFs in a diverse network of brain areas, consistent with previous studies (Culham et al., 2001; Jovicich et al., 2001; Shim et al., 2010; Jahn et al., 2012; Alnæs et al., 2014). Crucially, we extended the canonical load-dependent ARFs to include the hemifield in which targets are tracked. Several brain regions in the visual system showed a strong hemifield preference. These areas exhibited a contralateral bias in their ARFs, such that the effect of tracking load was stronger for contralateral than ipsilateral targets. Processing in these areas could be a cause of the hemifield-specific bottleneck in attentional tracking capacity seen behaviorally (Alvarez and Cavanagh, 2005; Holcombe and Chen, 2012; Störmer al., 2014). These areas were found bilaterally throughout the dorsal visual stream, including V3a, hMT, IPS, and SPL. In contrast, some higher-order attention–related areas, like the frontal and supplementary eye fields and subsets of the IPS, were modulated by targets regardless of their position in the visual field. For example, parts of the dorsal attention network in the parietal and frontal lobes responded to ipsilateral targets as well as to contralateral targets. Against Mesulam's (1981) hypothesis, we did not find evidence that the right hemisphere directs attention in a "more global" fashion than the left hemisphere.

Materials and Methods

Participants. We conducted an a priori power analysis based on the effect sizes reported in the literature on ARFs (Jovicich et al., 2001; Alnæs et al., 2014) using G*Power (Faul et al., 2007). This analysis revealed that one would need ~10 participants to detect ARFs with >90% power using an experimental design similar to these previous studies. A general recommendation based on simulations suggests the use of 20 participants when investigating strong, localized effects in fMRI as we do here (Cremers et al., 2017).

We therefore recruited 20 volunteers to participate in the experiment (10 men and 10 women). Their ages ranged from 20 to 60, with an average age of 28.8 years. Three authors (M.R.M, E.C., and P.T.) were among the participants. All participants gave informed consent and were reimbursed for their time with $30. Participants' vision was normal or corrected to normal. One participant was excluded from all analyses following an incidental finding in their structural MRI scan, which was referred to a neurologist. All procedures followed standard ethical guidelines and were approved by Dartmouth's Institutional Review Board.

Experimental design. As in other attentional tracking tasks, participants were instructed to maintain their attention on one or several target objects among physically identical distractors as these objects moved over the screen. At the beginning of every trial, eight circles with a diameter of 0.5 degrees of visual angle (dva) appeared on a black background, four of them in each hemifield. Between zero and four circles were highlighted in red to mark them as targets to be tracked, while distractor circles were highlighted in blue. Then all circles' colors reverted to white, and they moved over the screen randomly. We instructed participants to covertly track the positions of all target circles (i.e., those previously highlighted in red) with their attention while fixating a white crosshair in the center of the screen. After the circles stopped moving, one circle was randomly highlighted, and participants responded

whether it was one of the targets or one of the distractors in a two-alternative forced choice format where 50% accuracy would correspond to random guessing. Figure 1 depicts a schematic of the task configuration.

The red and blue colors marking some circles as targets and others as distractors were displayed for 2 s. After the circles turned white, they moved over the screen for 10 s. When the circles stopped moving, participants were given up to 5 s to respond whether the randomly highlighted circle had been a tracked target or a distractor. There was a 16 s break between trials (i.e., blocks) to allow the BOLD signal to return to the baseline.

This fMRI experiment was carried out as a block design. During each 17 s trial, the same number of objects moved across the screen. Between blocks (i.e., during the 16 s break), the screen was completely black. On a given trial, participants tracked between zero and four targets spread across the two hemifields (left, right) in nine possible load conditions as follows: (0,0), (0,1), (0,2), (1,0), (1,1), (1,2), (2,0), (2,1), (2,2). Objects that were not designated as targets in the beginning of a trial served as distractors. This way, the visual input to a participant's brain was identical during all tracking trials. Any difference in BOLD activity across experimental conditions must therefore have been caused by differences in processing rather than differences in the stimulus.

All circles translated over the screen in random directions at a speed of 1.75 dva/s. Shim et al. (2010), as well as others (Franconeri et al., 2008; Franconeri et al., 2013; Holcombe, 2023), have demonstrated that there is a strong interaction between load capacity and target speed, with slower object motion increasing the number of trackable targets. We kept object speed constant in all conditions and chose a speed that would allow most participants to track accurately at all tested tracking loads (Franconeri et al., 2008).

Motion directions were random but constrained in several ways. The objects moved within squares of 7 by 7 dva that were offset to the left and right of fixation by 2.5 dva, respectively, leading to a 5 dva minimum separation between the left and right hemifield areas of object motion. If their direction of motion would place them outside of the boundaries of these squares, their direction was changed randomly to a direction that would keep them inside their virtual boundary. Objects also maintained a minimum separation of 0.5 dva from each other and changed direction randomly when their object buffer zones collided.

The number of targets varied from zero to two targets in each hemifield, with all possible combinations across hemifields. Thus, the total tracking load ranged from zero to four targets. In this way, we were able to manipulate tracking load independently in each hemifield, leading to nine experimental conditions. In other words, every possible number of targets (zero to two) in one hemifield was paired with every possible number of targets in the other hemifield in a random order. A trial of each condition was included in every fMRI imaging run, and runs were repeated 10 times per participant (however, due to technical difficulties, two participants only completed eight and nine runs, respectively).

Stimulus presentation. Stimuli were created using MATLAB (MathWorks), specifically Psychophysics Toolbox (Brainard, 1997; Pelli, 1997). They were then projected onto a screen (19 dva by 7 dva projection area) inside the MRI scanner bore. Participants responded via button presses and were instructed to use the same finger to press the buttons throughout the experiment. Eye movements were recorded using an Eyelink 1000+ (SR Research) that was placed inside the scanner bore underneath the screen.

MRI acquisition. Images were acquired at the Dartmouth Brain Imaging Center on a 3 T Siemens PRISMA scanner. After a brief localizer scan, three-dimensional fieldmaps were collected (anterior to posterior and posterior to anterior), which were used for image preprocessing to aid with distortion correction. After the first five functional imaging runs [multiband T2* echoplanar imaging (EPI): TR, 1,000 ms; TE, 30 ms; resolution, 2 mm³ isotropic; flip angle, 60°; multiband factor, 4; Grappa, 2], we acquired a high-resolution T1 image (MPRAGE; resolution, 0.94 mm³ isotropic; flip angle, 8°; TR, 2.3 s; TE, 2.3 ms). This was then followed by the remaining five functional runs.

MRI preprocessing with fMRIPrep. Results included in this manuscript are based on data preprocessing performed using *fMRIPrep* 22.0.1 (Esteban et al., 2019), which is based on *Nipype* 1.8.4 (Gorgolewski et al., 2011). These tools print out a boilerplate description of processing steps detailing what methods, algorithms, and software packages were used with which recordings. This text is reprinted here:

A *fieldmap* was estimated based on two EPI references with *topup* (Andersson et al., 2003). The T1-weighted (T1w) image was corrected for intensity nonuniformity with *N4BiasFieldCorrection* (Tustison et al., 2010), distributed with ANTs 2.3.3 (Avants et al., 2008), and used as T1w reference throughout the workflow. The T1w reference was then skull-stripped with a *Nipype* implementation of the antsBrainExtraction.sh workflow (from ANTs), using OASIS30ANTs as target template. Brain tissue segmentation of cerebrospinal fluid, white matter, and gray matter was performed on the brain-extracted T1w using *fast* (FSL 6.0.5.1:57b01774; Zhang et al., 2001). Brain surfaces were reconstructed using recon-all (FreeSurfer 7.2.0; Dale et al., 1999), and the brain mask estimated previously was refined with a custom variation of the method to reconcile ANT-derived and FreeSurfer-derived segmentations of the cortical gray matter of *Mindboggle* (Klein et al., 2017). Volume-based spatial normalization to one standard space (MNI152NLin2009cAsym) was performed through nonlinear registration with antsRegistration (ANTs 2.3.3), using brain-extracted versions of both T1w reference and the T1w template.

For each of the 10 BOLD runs per participant, the following preprocessing was performed. First, a reference volume and its skull-stripped version were generated using a custom methodology of *fMRIPrep*. Head-motion parameters with respect to the BOLD reference (transformation matrices and six corresponding rotation and translation parameters) were estimated before any spatiotemporal filtering using mcflirt (FSL 6.0.5.1:57b01774; Jenkinson et al., 2002). The estimated *fieldmap* was then aligned with rigid registration to the target EPI reference run. The field coefficients were mapped on to the reference EPI using the transform. BOLD runs were slice-time corrected to 0.456 s (0.5 of slice acquisition range 0–0.912 s) using 3dTshift from AFNI (Cox and Hyde, 1997). The BOLD reference was then coregistered to the T1w reference using bbregister (FreeSurfer) which implements boundary-based registration (Greve and Fischl, 2009). Coregistration was configured with six degrees of freedom. The BOLD time series were resampled into standard space, generating a preprocessed BOLD run in *MNI152NLin2009cAsym space*. A reference volume and its skull-stripped version were generated using a custom methodology of *fMRIPrep*. The BOLD time series were resampled onto the following surfaces (FreeSurfer reconstruction nomenclature): *fsnative* and *fsaverage*. Surface resamplings were performed using mri_vol2surf (FreeSurfer).

Further MRI preprocessing. Functional data were spatially smoothed by iteratively averaging neighboring vertices, with a full-width at half-maximum (FWHM) of four vertices. Note that since smoothing was done in surface space, and due to the spatial nonuniformity of FreeSurfer's meshes (Ma et al., 2023), the FWHM of the smoothing procedure needs to be specified in terms of the lattice instead of millimeters.

An analysis using predefined parcellations of the brain can be used as an alternative to whole-brain group analyses. Such ROI analyses can reveal region-wide effects that would otherwise get drowned out on the vertex level. Additionally, comparing the brain hemispheres to each other at the vertex or voxel level should be avoided because brain hemispheres are asymmetric. ROIs make it possible to compare functionally equivalent areas between hemispheres. Finally, ROIs offer a more nuanced perspective on the clusters found in the whole-brain analyses, since the exact extent of these clusters depends among other things on choices like the cluster forming threshold. An ROI analysis sacrifices some spatial resolution but increases power and can reveal whether contralateral bias also exists outside the clusters identified in the whole-brain analysis.

Typically, ROIs are defined individually for each participant, using a functional localizer or retinotopic mapping. This has the benefit of

factoring in individual variability in the size and location of functionally distinct regions, so that this variability does not negatively impact the group-level analysis (Saxe et al., 2006). Recent findings have shown, however, that a large proportion of the interparticipant variability in the region size and location is closely tied to variability in the anatomy of the cortical surface. Surface-based normalization approaches allow for comparisons across participants that take this variability into account and factor in folding geometry of the cortical surface (Brodoehl et al., 2020). This has led to the rise of probabilistic atlases, based on surface-based group–level comparisons of ROI data from a large number of participants, that generalize well to new participants (Wang et al., 2015), even for higher-level visual regions (Rosenke et al., 2021). These atlases are extremely useful because they can be applied to new participants without the need for collecting retinotopy or functional localizer data in a separate fMRI session. The only thing necessary is acquiring an anatomical scan and running FreeSurfer's segmentation and surface reconstruction algorithm (Dale et al., 1999). Here we used ROIs based on a probabilistic atlas of topographically organized visual areas, created by Wang et al. (2015). This atlas was generated by functionally defining 25 topographic ROIs covering 22 visual areas in ∼50 individual participants, standardizing each participant's cortical surface using icosahedral tessellation and projection (Argall et al., 2006) and then assessing the likelihood, across participants, of each vertex on the standardized surface belonging to a particular ROI. The atlas was defined using a maximum probability approach, which only considers a given vertex as part of the set of ROIs if it is more often found within the set than outside the set, across participants. If this is the case, the vertex is given the value of the most likely ROI. This approach captures much of the overall structure of ROIs defined for individual participants and generalizes well to novel participants who did not contribute to the atlas' generation (Wang et al., 2015). We downloaded the atlas from https://napl.scholar.princeton.edu/resources and converted the ROIs from the standardized surface space to FreeSurfer native space (fsnative) for each of our participants, using a script created by Takamura and Benson, also available at the link above. We excluded five ROIs from our analysis, IPS4 and 5, SPL, TO2, and FEF, each of which covered a comparatively small number of vertices in the probabilistic atlas, due to high variability in their location across participants. The dorsal and ventral segments of V1, V2, and V3 were analyzed separately. The result was a total of 20 ROIs in each hemisphere, shown in outline in Figure 2.

Statistical analyses. Tracking accuracy was assessed statistically using mixed-effect binomial logistic regression models fitted to binary outcome data. The model included fixed effects for the number of targets on the left and on the right, along with a random effect for individual participants. To assess the significance of target loads on tracking accuracy, we compared the model with two nested alternative models, each excluding either the predictor for left or right load, using likelihood ratio tests (Luke, 2017). This approach allowed us to estimate how adding targets to each hemifield affected tracking accuracy while controlling for the number of targets in the other hemifield. Similarly, eye movement data were analyzed using mixed-effect models to evaluate differences in gaze behavior between conditions.

To analyze the fMRI data, we first fit a generalized linear model (GLM) to BOLD time series data from all runs at each vertex in fsaverage space, with nine regressors of interest estimating brain responses to each experimental condition separately. Besides the regressors for each condition, we used nuisance regressors for motion (six rigid motion directions estimated during preprocessing) and for scanner drift (first- and second-order polynomials). The resulting beta maps were then used for all group-level whole–brain analyses.

At the group level, we fit linear mixed models at each vertex to the beta maps generated for each participant and condition, described below in Wilkinson notation (Wilkinson and Rogers, 1973). The effect of total load as well as the comparison of tracking against passive viewing (Fig. 2) can be estimated from the following model:

$$\% \text{ signal change } \sim \text{load}_{\text{total}} + (1|\text{participant}),$$

where (1|participant) indicates the random effect for each participant, while effects of hemifield-specific load (Fig. 3) were estimated similarly using a model of the following form:

$$\% \text{ signal change } \sim \text{load}_{\text{left}} + \text{load}_{\text{right}} + (1|\text{participant}).$$

Contrast images were smoothed by iteratively averaging neighboring vertices. All statistical analyses were conducted in surface space. This approach improves the signal-to-noise ratio and accounts better for individual differences in brain anatomy than smoothing in volume space (Brodoehl et al., 2020).

Whole-brain analyses involve statistical tests at each vertex and therefore require correction for multiple comparisons (Bennett et al., 2009). To this end, we used random field theory, which estimates the probability of finding a cluster of vertices with a certain height empirically from the smoothness of the image by accounting for the spatial autocorrelation of fMRI data (Worsley, 2001; Chung et al., 2010). The data were then cluster corrected using random field theory with an initial cluster forming threshold of $p < 0.0001$. These analyses were implemented using the python packages *Nilearn* (version 0.10.0) and *BrainStat* (0.4.2). We used *Nilearn* for visualizations.

The same GLM was fit to the data in fsnative space for the atlas-based (Wang et al., 2015) ROI analysis to estimate the ARF slopes and intercepts directly from the ROIs' mean percentage signal change. To estimate the impact of an added target on brain activity, linear regression models were individually fitted for each participant, hemisphere, and ROI, regressing the signal change within each ROI against the number of targets in each hemifield. This enabled the estimation of individual ARF slopes, representing changes in BOLD signal per additional target, while controlling for variations in the number of targets in the opposite hemifield. This analysis isolates and quantifies the unique contribution of ipsilateral and contralateral loads to the BOLD response across different ROIs and hemispheres. Crucially, an ROI analysis allows for a systematic comparison of the two hemispheres, because ROIs can provide meaningful corresponding units for hemispheric comparison unlike a direct vertex-to-vertex comparison.

Following the individual estimation of ARF slopes, we applied separate linear mixed-effect models for each type of load (contralateral and ipsilateral) to assess whether homologous ROIs across the two hemispheres differed in their response to changes in contra- and ipsilateral load. These models included fixed effects for ROIs and hemispheres, as well as their interaction, and a random effect for participants. We assessed the significance of interaction effects by comparing these models to nested models without the interaction term (Luke, 2017). Upon identifying significant interactions, post hoc *t* tests on estimated marginal means were performed, with Bonferroni's correction applied for multiple comparisons.

Results

Tracking accuracy

Participant performance was near ceiling across all conditions, with an overall mean accuracy of 91.26% (SD, 5.28; chance performance, 50%). Performance decreased significantly as the target load increased in both hemifields. These effects were assessed using mixed-effect binomial logistic regression models, incorporating fixed effects for the number of targets on each hemifield and a random effect for participants. The model was compared against two nested alternative models that excluded either the left load or right load predictor, using likelihood ratio tests (Luke, 2017). The results revealed that load in both hemifields had a significant effect on accuracy during multiple-object tracking (left, $\chi^2_{(1)} = 22.54$; $p < 0.001$; right, $\chi^2_{(1)} = 6.45$; $p = 0.011$). The model estimated a decrease in accuracy of 2.17% with the addition of the first target in the left hemifield and a further decrease of 3.71% with the addition of the second target. In the right hemifield, accuracy decreased by 0.97% for the first additional target and by 1.28% for the second. We also examined potential interaction between hemifields by adding an interaction term

into the model, yet the test identified no significant difference ($\chi^2_{(1)} = 0.42$; $p = 0.516$). Average performance in each condition, as well as trend lines showing the decrease in accuracy with higher load are depicted in Figure 1D.

Eye movements

Due to technical difficulties with the eye tracking equipment, only 17 of the 20 participants' data were included in the analysis of eye movements. To verify that participants were fixating properly,
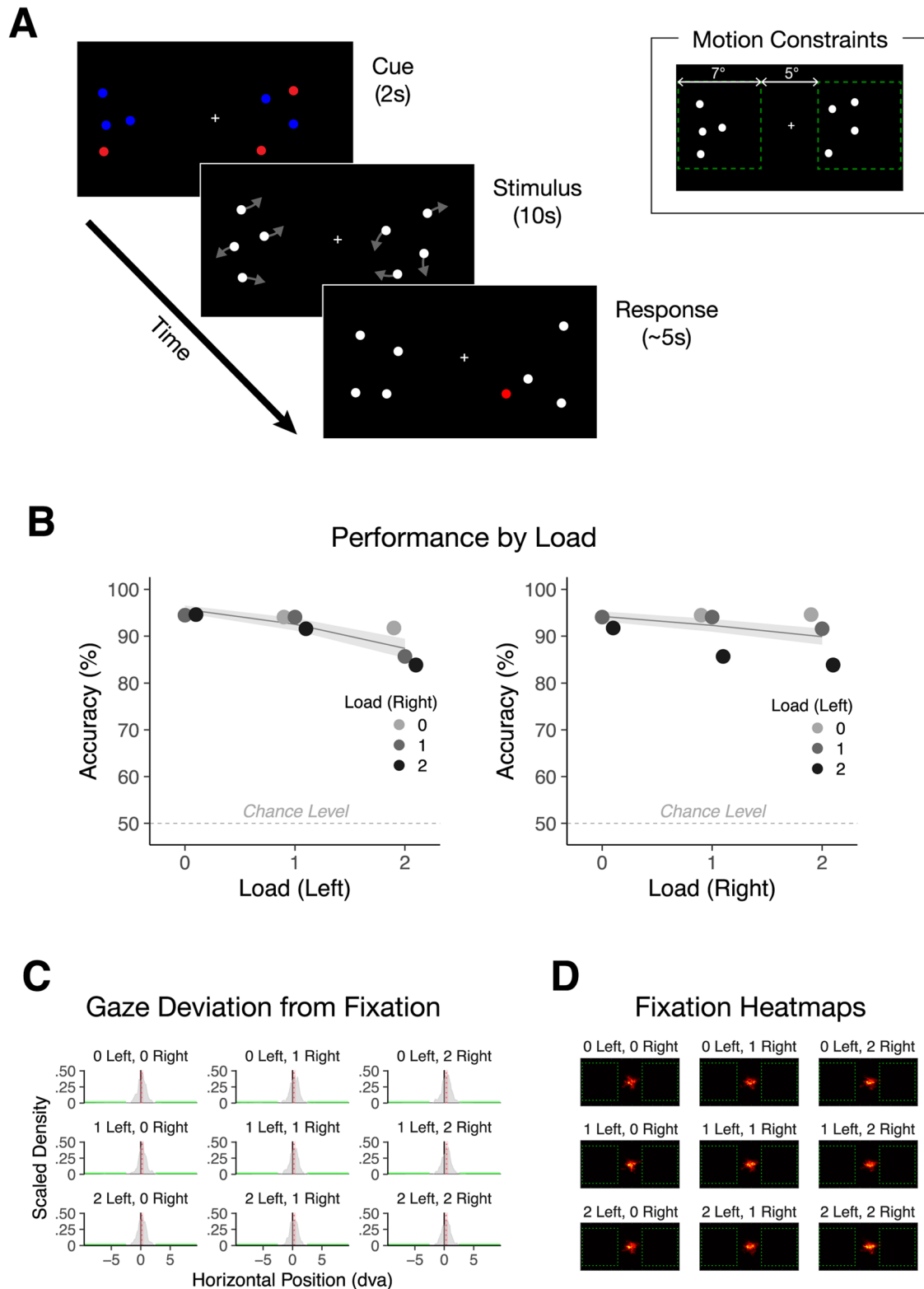

Figure 1. Task and task performance. **A**, Schematic diagram of the stimuli. **B**, Accuracy in the task decreased with increasing load (i.e., task difficulty). Data points have been slightly shifted horizontally for visibility. **C**, Results of the eye tracking analysis showing horizontal deviations of gaze from the fixation point during the task. Participants were instructed to fixate a cross in the center of the screen. Participants were looking at the area where the targets were presented (green x-axis labels) for ~1% of the time. **D**, Heatmaps showing where participants' gaze was concentrated in each condition.

their eye movements were recorded while they performed the task inside the scanner. To quantify the deviation of gaze from the fixation to the target area, we analyzed the density distributions of horizontal gaze positions, normalized and averaged across participants (Fig. 1C,E). Mean gaze position and 95% confidence intervals were estimated using a linear mixed-effect model, incorporating subject-specific intercepts as random effects. Across conditions, recorded eye gaze remained close to the fixation cross, with participants spending an average of 0.93% of the trial duration (SD, 2.22, SE, 0.18; CI, [0.58, 1.28]) fixating on the target area. A quasi-binomial GLM revealed no significant effect across conditions on target fixation time ($\chi^2_{(8)} = 2.63$; $p = 0.956$), indicating that gaze allocation remained stable across conditions.

Spatial attention can bias fixational eye movements (Engbert and Kliegl, 2003). To characterize the maximal degree to which the spatial distribution of targets might have influenced fixations, we fit Gaussian distributions to the mean heatmap (Fig. 1D) of each participant and condition and compared their means. Trials with high load in one hemifield and no targets in the other hemifield should show the strongest bias in fixational eye movements if this bias was caused by imbalances in load. During trials with two targets on the left and zero targets on the right side of the screen, participants fixated significantly more toward the left compared with trials with two targets on the right and none on the left ($t_{(16)} = 2.54$; $p = 0.022$). While this post hoc test to the aforementioned GLM reached significance, the mean difference was only 0.168 dva, with a 95% confidence interval between 0.03 and 0.3 dva. Based on this, we conclude that the fraction of fixations on the targets (<1%) and the difference in fixation locations between conditions were so small that no further corrections for eye movements were necessary.

Tracking-related brain activity
In line with previous studies (Culham et al., 2001; Alnæs et al., 2014), we first calculated a linear contrast comparing tracking any number of targets to passive viewing of the same stimuli (i.e., no targets in either hemifield), revealing the "task areas" depicted in Figure 2A. We found clusters of vertices in both the dorsal attention network and the ventral attention network (Fiebelkorn and Kastner, 2020) which reacted much more strongly to the task than to passive viewing of the stimuli. Consistent with what has been shown previously (Culham et al., 2001; Jovicich et al., 2001; Shim et al., 2010; Jahn et al., 2012; Alnæs et al., 2014; Nummenmaa et al., 2017), we found strong and widespread activations in the occipital, parietal, and frontal lobes.

Modulation by total attentional load
Before assessing hemifield preference in ARFs, it was necessary to show that we found the canonical ARFs (Culham et al., 2001; Jovicich et al., 2001; Shim et al., 2010; Jahn et al., 2012; Alnæs et al., 2014; Nummenmaa et al., 2017). A wide array of brain areas showed parametric modulation of activity depending on the total number of tracked targets (Fig. 2B). Significant clusters of activations were found in the dorsal visual stream (including but not limited to V3a, V3b, hMT), as well as the dorsal and ventral attention network, IPS, SPL, FEF, and the anterior insula. The activations were essentially bilateral with slightly larger clusters in the right hemisphere. Additionally, areas, where activity was modulated by the number of tracked targets, were a subset of the task areas (compare Fig. 2A,B).

Modulation by contralateral and ipsilateral load
After establishing that our data replicate the canonical ARF findings, we sought to investigate whether this effect is driven by targets bilaterally or whether ARFs show hemifield-specific effects like other aspects of multiple-object tracking (Alvarez and Cavanagh, 2005; Holcombe and Chen, 2012; Störmer et al., 2014). We found that contralateral load varies with brain activity throughout the dorsal visual stream, as well as the dorsal attention network. Activation maps were largely overlapping for parametric modulation with total load and with contralateral load (compare Figs. 2 and 3). Ipsilateral load on the other hand also showed clusters where BOLD was modulated significantly, but these clusters emerged much later in the visual processing stream and were largely in attention-related frontal and parietal areas like IPS and the supplementary eye fields.

Contralateral preference
Areas where BOLD activity was more strongly modulated by contralateral than ipsilateral target tracking load were revealed by directly contrasting the beta maps corresponding to modulation with targets on the left and right with each other (Fig. 3C). In both hemispheres, clusters in the dorsal visual stream (V3a/b, hMT) showed stronger modulation with contralateral than with ipsilateral load. Additionally, there were clusters in the SPL in both hemispheres, with larger clusters in the right hemisphere.

ROIs
By fitting a linear regression to the ROI data from each experimental condition, we can estimate the relationship between the BOLD signal and the number of targets in each hemifield. Specifically, the slope of this fit line is the increase (or decrease) in percentage signal change caused by one added target in a specific hemifield while controlling for load in the other hemifield. This allowed us to determine the extent to which BOLD increases with each additional target, separately for each hemifield and hemisphere. Examples of this analysis for two ROIs are shown in Figure 4A.

Consistent with the results of the whole-brain analysis, there were contralateral ARFs with slopes significantly greater than zero in many ROIs throughout the dorsal and ventral visual stream (Fig. 4). Similarly, evidence of increased BOLD with additional ipsilateral targets emerged later in the visual hierarchy, in the IPS.

To determine if contra- and ipsilateral ARF slopes differed between hemispheres, we assessed interaction effects between ROIs and hemispheres for each type of ARF. Our linear mixed-effect models, incorporating fixed effects for ROIs and hemispheres and their interactions, were compared against nested models that excluded the interaction terms. The model comparison revealed a significant interaction for ipsilateral targets ($\chi^2_{(19)} = 43.27$; $p = 0.001$), whereas no significant interactions were found for contralateral targets ($\chi^2_{(19)} = 16.53$; $p = 0.621$). Post hoc t tests on estimated marginal means, corrected for multiple comparisons using the Bonferroni method, were performed for ipsilateral ARFs to explore differences between hemispheres within each ROI. These pairwise comparisons across hemispheres for each ROI are presented in detail in Figure 4D.

Discussion
Our study is the first fMRI-based investigation of hemifield- and hemisphere-specific effects in ARFs during multiple-object tracking. Increases in the number of tracked targets during multiple-object tracking led to increases in activity throughout the visual system and the dorsal and ventral attention networks (Fig. 2). Crucially, for many of the load-sensitive brain regions
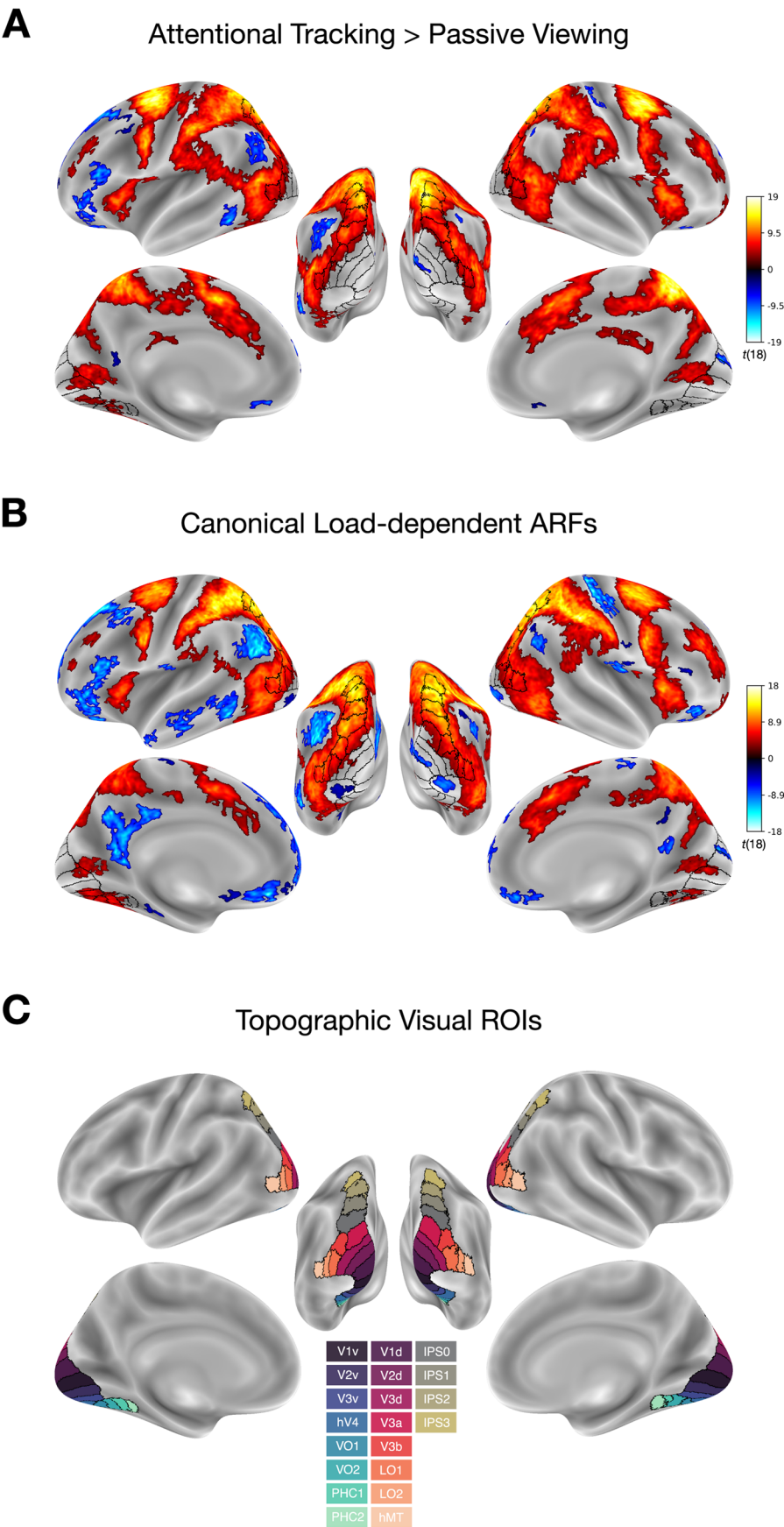
Figure 2. Canonical ARFs. Task (*A*) and load-dependent (*B*) ARFs projected onto FreeSurfer's fsaverage surface mesh. *C*, The ROIs outlined on brains in *A* and *B* are from a probabilistic atlas by Wang et al. (2015).

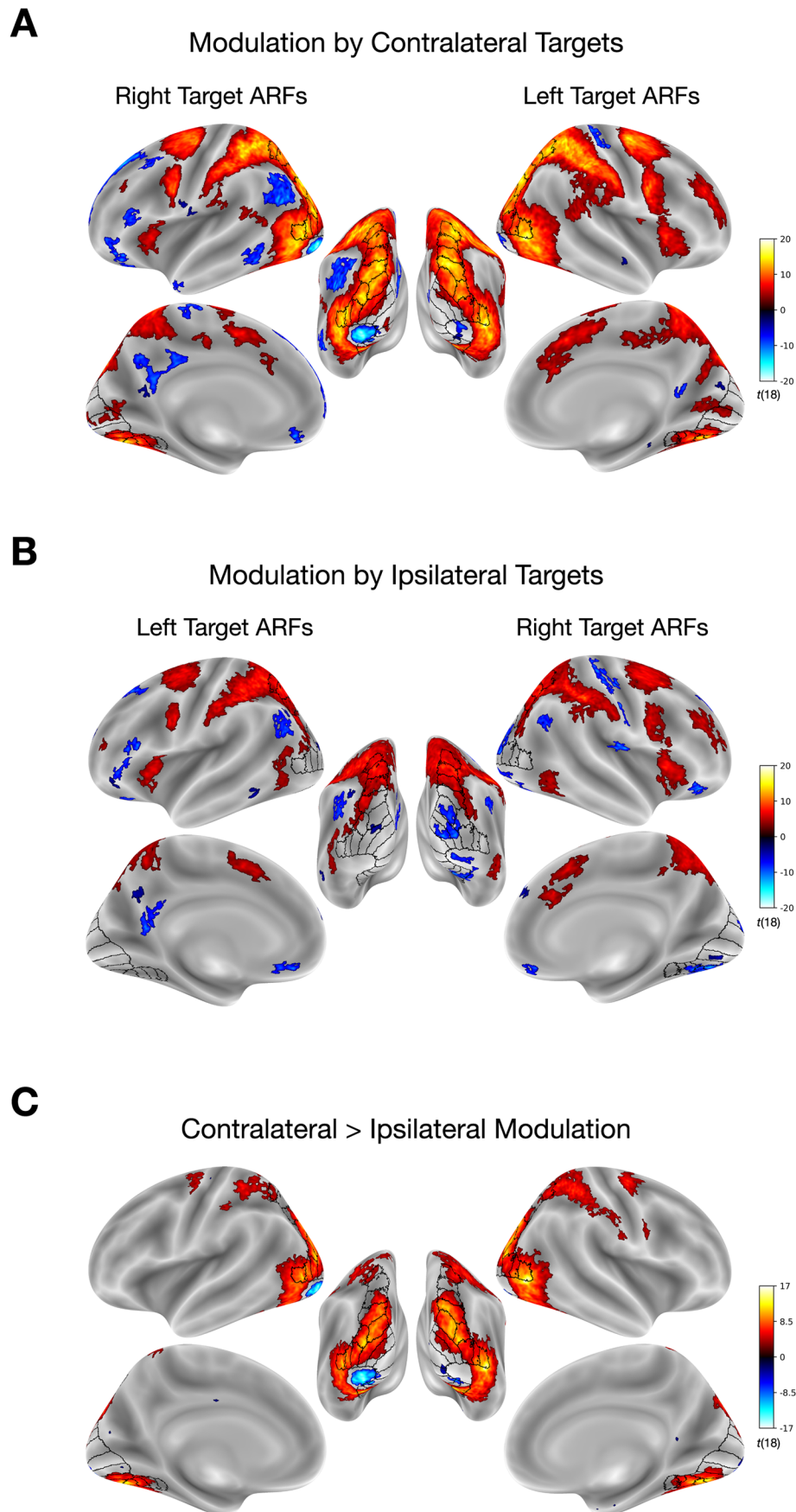**Figure 3.** Hemifield-dependent ARFs. Contralateral (*A*) and ipsilateral (*B*) ARFs as well as their direct comparison (*C*). Overlayed ROIs are the same as in Figure 2.
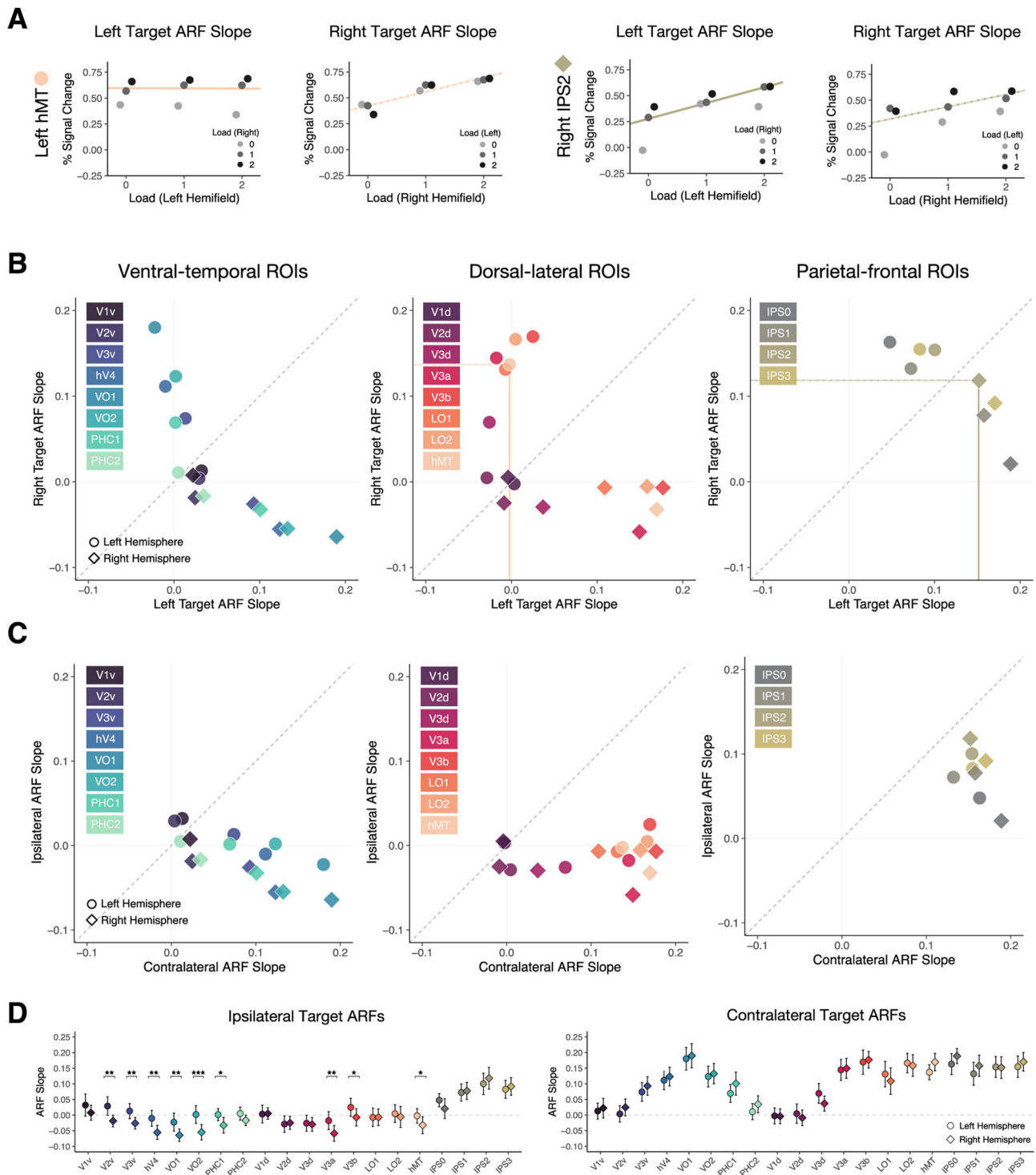
Figure 4. ROI analyses. **A**, ARF slopes were computed for each ROI by fitting first-order polynomials to the activity caused by the number of left or right targets. The slope of this line is the average increase in activity caused by increasing the number of targets. Left hMT shows a modulation of its response by right load, but not by left load, while right IPS2 shows a response to changes in load on both sides. Data points have been slightly shifted along the load axis for visibility. **B**, Comparing the slope of the ARFs for left and right targets in each ROI. We use a threefold separation of the ROIs for plotting purposes, inspired by the original presentation of the ROIs (Wang et al., 2015). We do this to reduce clutter in our plots and do not intend to imply functional distinctions among the ROIs. **C**, The same data as (**B**) but organized additionally by the spatial relationship between hemifields and ROIs. This makes it possible to compare the slope of ARFs with contra- and ipsilateral targets in each ROI. **D**, Directly compares corresponding ROIs from each hemisphere. While there was no difference between the hemispheres in their response to contralateral targets, some right hemisphere ROIs showed a significant negative ARF slope in response to increases in ipsilateral load. Left hemisphere ROIs are indicated with circles, right hemisphere ROIs with diamonds. Asterisks indicate significant, pairwise, Bonferroni-corrected differences between equivalent ROIs from the two hemispheres, independent of their difference from a baseline slope of zero. Error bars correspond to the 95% confidence intervals around the estimated slope.

in both hemispheres, this response was dependent on the hemifield in which the target was added (Fig. 3A,B), and a subset of those areas were significantly more modulated by contra- than

ipsilateral load (Fig. 3C). While activity in early visual areas was modulated exclusively by contralateral load, both contralateral and ipsilateral load modulated activity in the frontoparietal

attention network. This suggests either that these areas are involved in attentional tracking of objects in both visual hemifields or that these areas engage in cross talk between the hemispheres that is relatively absent in earlier visual processing areas. ROI analyses further showed a transition from early to late areas in the visual processing hierarchy. Specifically, early areas have a strong contralateral bias whereas later areas do not; their activity is modulated by both ipsi- and contralateral tracking load (Fig. 4). These later areas are part of the frontoparietal attention network and have previously been found to be active during multiple-object tracking (Alnæs et al., 2014) but also in paradigms targeting other aspects of attention (Fiebelkorn and Kastner, 2020). Both hemispheres showed similar patterns of ARFs to contra- and ipsilateral load. We found no evidence for Mesulam's (1981) hypothesis that the right hemisphere attentional system processes more "globally" than the left's. The only exception to this functional symmetry was that right hemisphere occipital ROIs showed a decrease in activity with increases in ipsilateral load that was not seen anywhere in the left hemisphere.

Most previous investigations of ARFs did not analyze whether targets were ipsi- or contralateral to the ROIs and so were unable to reveal the hemifield-specific processing in earlier visual areas that we find here. The only previous study to include this kind of analysis (Shim et al., 2010) did not find statistically significant hemifield effects, perhaps because they only varied the number of targets between one and two. Our findings validate investigations into ARFs (Culham et al., 2001; Jovicich et al., 2001; Shim et al., 2010; Jahn et al., 2012; Alnæs et al., 2014) and extend our understanding of ARFs to include hemifield and hemisphere specificity.

Our findings also bridge electrophysiological findings of load-dependent increases of steady-state visual evoked potentials in EEG electrodes over occipital areas (Störmer et al., 2013; Störmer et al., 2014; Adamian and Andersen, 2022) with previous fMRI experiments showing load-dependent activity mostly in parietal and frontal areas (Culham et al., 2001; Jovicich et al., 2001; Shim et al., 2010; Jahn et al., 2012; Alnæs et al., 2014). Our data are consistent with these findings and provide new evidence indicating that higher-level areas in IPS and SPL are involved in contralateral processing. Our results also support and extend previous results showing that contra- and ipsilateral targets influence BOLD activity in parietal lobe ROIs (Shim et al., 2010).

Overall, we observed larger clusters and stronger effects in the right hemisphere. However, this needs to be interpreted with caution, because the hemispheres are not structurally symmetric. A more appropriate comparison of the left and right hemispheres can be accomplished using ROIs that map functional equivalents across the two hemispheres (Wang et al., 2015). When comparing the left and right hemispheres, we found one consistent difference: several ROIs in the right hemisphere show a negative ARF (decreasing activity) with increasing ipsilateral load. In other words, as the left hemisphere increases its tracking efforts, the right hemisphere shows a relative decrease in BOLD response. Future modeling efforts will be necessary to connect this effect with existing findings of hemispheric and hemifield imbalances of attentional processing (Posner and Petersen, 1990; Petersen and Posner, 2012; Hoyos et al., 2021).

The most prominent lateralization of the attention system is revealed by hemispatial neglect, which occurs much more frequently after right parietal stroke than left parietal stroke. Several explanations for this asymmetry have been suggested (Heilman and Van Den Abell, 1980; Mesulam, 1981; Kinsbourne, 1987;

Parton et al., 2004; Corbetta and Shulman, 2011; Duecker and Sack, 2015; Esposito et al., 2021). Theoretical accounts of neglect propose different degrees of hemispheric contralateral bias for spatial attention. One theory proposes that the left hemisphere controls attentional shifts toward the right hemifield, while the right hemisphere controls attentional shifts toward both hemifields. A competing account claims that each hemisphere has a contralateral bias for attentional shifting but also represents the ipsilateral hemifield (Heilman and Van Den Abell, 1980; Mesulam, 1981; Corbetta and Shulman, 2011; Szczepanski and Kastner, 2013; Duecker and Sack, 2015). Our data reveal a contralateral bias in both hemispheres, as well as responses to ipsilateral targets in both hemispheres, so are more consistent with the latter theory. The decrease in activity with increases in ipsilateral load that is observed in right hemisphere ROIs might also be related to or caused by this interhemispheric competition. Negative ARFs during tracking have been found in brain areas that process vestibular inputs (Frank et al., 2016), which coincides with decreases of glutamate and glutamine in those areas (Frank et al., 2021). Future spectroscopy experiments could determine whether the negative ARFs we report here are also related to such changes in neurotransmitter concentrations in right visual ROIs. The presented experiment, however, is not suited well for revealing competition between hemispheres and is based on findings showing hemispheric resource independence (Alvarez and Cavanagh, 2005; Holcombe and Chen, 2012; Hudson et al., 2012; Störmer et al., 2014).

Right hemisphere dominance has also been reported in investigations of healthy attention systems. Posner and Petersen (Posner and Petersen, 1990; Petersen and Posner, 2012) proposed a taxonomy for spatial attention that is segregated into orienting, alertness, and executive control. In their review paper (Petersen and Posner, 2012), they also note that many studies have found aspects of spatial attention to be right-lateralized in the brain. Leftward biases in spatial attention are common among young children but through development these biases become weaker (Hoyos et al., 2021). Contralateral biases in visual processing have also been investigated in the context of visuospatial working memory, which likely shares mechanisms with spatial attention. While some experiments find contralateral biases during lateralized working memory tasks in both hemispheres (Killebrew et al., 2015), others find contralateral bias only in the left hemisphere (Sheremata et al., 2010).

Another kind of hemispheric specialization for multiple-object tracking has been proposed by Merkel and colleagues (Merkel et al., 2015; Merkel et al., 2024). Their hypothesis distinguishes between tracking the locations of each individual target as opposed to tracking the shape of an illusory polygon, the vertices of which are the locations of the targets. There is some evidence indicating a left hemifield, right hemisphere dominance of the shape-based tracking strategy (Merkel et al., 2024). While these findings are intriguing, our study was not designed to distinguish between these two strategies. Our results focused on where the tracking processes occurred not how, and our conclusions are independent of the mechanisms involved.

In addition to hemifield biases, attention is also characterized by relative hemifield independence in tracking capacity. Specifically, the capacity for multiple-object tracking and the maximum speed of trackable objects both nearly double when targets are spread across hemifields rather than being limited to one hemifield (Alvarez and Cavanagh, 2005; Holcombe and Chen, 2012; Hudson et al., 2012; Störmer et al., 2014). Hemifield-specific effects are not observed in tasks where the

primary cognitive effort is undertaken by higher-order regions without hemifield-specific representations (Luck et al., 1989; Duncan et al., 1999). In particular, capacity and speed limits would not show hemifield specificity if the tracking limit were imposed in higher-level areas because we find that these areas respond to targets bilaterally. Based on our results, we conjecture that the areas with contralateral preference that we found in the visual system (e.g., V3a/b and hMT) are likely primarily responsible for the overall tracking limits found in behavioral studies. If later bilateral areas significantly constrained tracking capacity, the advantage would necessarily be less than a factor of two.

This can be further demonstrated using multiple-identity tracking, which is similar to multiple-object tracking but with the added requirement to also keep track of which target is which. Hemifield-specific effects are less pronounced in multiple-identity tracking, and the capacity limit is dramatically lower (Hudson et al., 2012). The capacity for multiple-object tracking nearly doubles when targets are spread across hemifields, but during multiple-identity tracking, the proportional increase is much smaller (Hudson et al., 2012; Holcombe, 2023). This suggests that the key processing bottlenecks for multiple-identity tracking, possibly related to working memory, are outside of the areas where multiple-object tracking activity shows contralateral bias. In comparison to multiple-object tracking, multiple-identity tracking also causes significantly more activation in the frontal lobe (Nummenmaa et al., 2017).

A common description of spatial attention involves "gain" or "saliency" maps that send feedback to sensory maps to enhance or suppress processing at relevant locations (Itti and Koch, 2001; Cavanagh et al., 2023). Load-sensitive areas may reflect activity in gain maps that represent the tracked targets as well as the consequences for sensory maps that receive feedback from gain maps. Task-dependent modulation of sensory maps in the occipital lobe might include changes to the properties of their population receptive fields, such as changes in their size and eccentricity (Grill-Spector et al., 2017). In either case, our results suggest that hemifield maps in the visual system underlie the capacity and speed bottlenecks. Such bottlenecks arise in these hemifield maps because the suppression surrounding each focus of attention interferes with nearby attentional selection (Mounts, 2000), and importantly, this attentional interference does not cross the vertical meridian (Carlson et al., 2007; Franconeri et al., 2013).

Our results suggest that regions in the occipital lobe where we found significantly stronger contralateral than ipsilateral ARFs (Fig. 3C) may serve as the primary source of attentional bottlenecks. These regions span both the dorsal and ventral visual streams, consistent with the dual demands of multiple-object tracking: segmenting objects from their background and tracking their motion. The involvement of both motion-sensitive and object-selective cortical areas aligns with these complementary processing requirements.

We propose that the capacity bottleneck for multiple-object tracking might arise in areas such as V3a (Caplovitz and Tse, 2007) and hMT where the modulation of activity with contralateral load was significantly stronger compared with ipsilateral load. However, we deliberately chose stimulus parameters that would allow participants to track four targets with high accuracy (Franconeri et al., 2008). Because of this, accuracy was near ceiling, and we observed no notable hemifield-specific capacity. With higher difficulty, we might have replicated hemifield-independent resources (Alvarez and Cavanagh, 2005; Holcombe, 2023). Nevertheless, such increased task demands would likely cause

participants to lose track of targets. To make reliable claims about the number of targets being tracked, it was crucial to ensure that participants would be genuinely capable of tracking that specific number of targets. Future experiments should include conditions with greater levels of difficulty that make it possible to link hemifield-specific capacity limits to brain activity. If our prediction holds, activity in the dorsal visual stream, where modulatory effects are significantly stronger for contralateral than ipsilateral targets, should reveal the relatively independent tracking limits of each hemifield. Specifically, we would expect that load-dependent ARFs show an increase in BOLD signal with the number of targets in the contralateral hemifield up to the capacity limit and then asymptote with more targets, to some extent independently of the number of targets in the other hemifield.

In conclusion, our study confirms and extends previous research on the neural correlates of multiple-object tracking. We find that brain activity in the visual, parietal, and frontal cortex is strongly modulated by the number of tracked targets and that many load-sensitive areas respond to targets in both hemifields. Furthermore, we identified a subset of load-dependent areas that exhibit a contralateral bias. Our findings suggest that these areas may be candidate regions for hemifield-specific limitations in attentional tracking performance, which then impose the bottleneck on tasks with bilateral target presentation. Capacity and speed limits would not be hemifield specific if the tracking limit were imposed in areas that respond to targets bilaterally. Overall, our findings shed light on the neural mechanisms underlying multiple-object tracking and provide insights into the hemifield- and hemisphere-specific effects of spatial attention.

References

Adamian N, Andersen SK (2022) Attentional enhancement of tracked stimuli in early visual cortex has limited capacity. J Neurosci 42:8709–8715.

Alnæs D, Sneve MH, Espeseth T, Endestad T, van de Pavert SHP, Laeng B (2014) Pupil size signals mental effort deployed during multiple object tracking and predicts brain activity in the dorsal attention network and the locus coeruleus. J Vis 14:1–1.

Alvarez GA, Cavanagh P (2005) Independent resources for attentional tracking in the left and right visual hemifields. Psychol Sci 16:637–643.

Andersson JL, Skare S, Ashburner J (2003) How to correct susceptibility distortions in spin-echo echo-planar images: application to diffusion tensor imaging. Neuroimage 20:870–888.

Argall BD, Saad ZS, Beauchamp MS (2006) Simplified intersubject averaging on the cortical surface using SUMA. Hum Brain Mapp 27:14–27.

Avants BB, Epstein CL, Grossman M, Gee JC (2008) Symmetric diffeomorphic image registration with cross-correlation: evaluating automated labeling of elderly and neurodegenerative brain. Med Image Anal 12:26–41.

Bennett CM, Miller MB, Wolford GL (2009) Neural correlates of interspecies perspective taking in the post-mortem Atlantic Salmon: an argument for multiple comparisons correction. Neuroimage 47:S125.

Brainard DH (1997) The psychophysics toolbox. Spat Vis 10:433–436.

Brodoehl S, Gaser C, Dahnke R, Witte OW, Klingner CM (2020) Surface-based analysis increases the specificity of cortical activation patterns and connectivity results. Sci Rep 10:5737.

Caplovitz GP, Tse PU (2007) V3a processes contour curvature as a trackable feature for the perception of rotational motion. Cereb Cortex 17:1179–1189.

Carlson TA, Alvarez GA, Cavanagh P (2007) Quadrantic deficit reveals anatomical constraints on selection. Proc Natl Acad Sci U S A 104:13496–13500.

Cavanagh P, Alvarez GA (2005) Tracking multiple targets with multifocal attention. Trends Cogn Sci (Regul Ed) 9:349–354.

Cavanagh P, Caplovitz GP, Lytchenko TK, Maechler MR, Tse PU, Sheinberg D (2023) The architecture of object-based attention. Psychon Bull Rev 30:1643–1667.

Chung MK, Worsley KJ, Nacewicz BM, Dalton KM, Davidson RJ (2010) General multivariate linear modeling of surface shapes using SurfStat. Neuroimage 53:491–505.

Corbetta M, Shulman GL (2011) Spatial neglect and attention networks. Annu Rev Neurosci 34:569–599.

Cox RW, Hyde JS (1997) Software tools for analysis and visualization of fMRI data. NMR Biomed 10:171–178.

Cremers HR, Wager TD, Yarkoni T (2017) The relation between statistical power and inference in fMRI. PLoS One 12:e0184923.

Culham JC, Cavanagh P, Kanwisher NG (2001) Attention response functions: characterizing brain areas using fMRI activation during parametric variations of attentional load. Neuron 32:737–745.

Dale AM, Fischl B, Sereno MI (1999) Cortical surface-based analysis: I. Segmentation and surface reconstruction. Neuroimage 9:179–194.

Duecker F, Sack AT (2015) The hybrid model of attentional control: new insights into hemispheric asymmetries inferred from TMS research. Neuropsychologia 74:21–29.

Duncan J, Bundesen C, Olson A, Humphreys G, Chavda S, Shibuya H (1999) Systematic analysis of deficits in visual attention. J Exp Psychol 128:450–478.

Engbert R, Kliegl R (2003) Microsaccades uncover the orientation of covert attention. Vision Res 43:1035–1045.

Esposito E, Shekhtman G, Chen P (2021) Prevalence of spatial neglect post-stroke: a systematic review. Ann Phys Rehabil Med 64:101459.

Esteban O, et al. (2019) fMRIPrep: a robust preprocessing pipeline for functional MRI. Nat Methods 16:111–116.

Faul F, Erdfelder E, Lang AG, Buchner A (2007) G* Power 3: a flexible statistical power analysis program for the social, behavioral, and biomedical sciences. Behav Res Methods 39:175–191.

Fiebelkorn IC, Kastner S (2020) Functional specialization in the attention network. Annu Rev Psychol 71:221–249.

Franconeri SL, Alvarez GA, Cavanagh P (2013) Flexible cognitive resources: competitive content maps for attention and memory. Trends Cogn Sci (Regul Ed) 17:134–141.

Franconeri SL, Lin JY, Enns JT, Pylyshyn ZW, Fisher B (2008) Evidence against a speed limit in multiple-object tracking. Psychon Bull Rev 15: 802–808.

Frank SM, Forster L, Pawellek M, Malloni WM, Ahn S, Tse PU, Greenlee MW (2021) Visual attention modulates glutamate-glutamine levels in vestibular cortex: evidence from magnetic resonance spectroscopy. J Neurosci 41: 1970–1981.

Frank SM, Sun L, Forster L, Peter UT, Greenlee MW (2016) Cross-modal attention effects in the vestibular cortex during attentive tracking of moving objects. J Neurosci 36:12720–12728.

Gorgolewski K, Burns CD, Madison C, Clark D, Halchenko YO, Waskom ML, Ghosh SS (2011) Nipype: a flexible, lightweight and extensible neuroimaging data processing framework in python. Front Neuroinform 5:13.

Greve DN, Fischl B (2009) Accurate and robust brain image alignment using boundary-based registration. Neuroimage 48:63–72.

Grill-Spector K, Weiner KS, Kay K, Gomez J (2017) The functional neuro-anatomy of human face perception. Annu Rev Vis Sci 3:167–196.

Heilman KM, Van Den Abell T (1980) Right hemisphere dominance for attention: the mechanism underlying hemispheric asymmetries of inattention (neglect). Neurology 30:327–327.

Holcombe AO (2023) *Elements in perception*. Cambridge, UK: Cambridge University Press.

Holcombe AO, Chen WY (2012) Exhausting attentional tracking resources with a single fast-moving object. Cognition 123:218–228.

Hoyos PM, Kim NY, Cheng D, Finkelston A, Kastner S (2021) Development of spatial biases in school-aged children. Dev Sci 24:e13053.

Hudson C, Howe PD, Little DR (2012) Hemifield effects in multiple identity tracking.

Intriligator J, Cavanagh P (2001) The spatial resolution of visual attention. Cogn Psychol 43:171–216.

Itti L, Koch C (2001) Computational modelling of visual attention. Nat Rev Neurosci 2:194–203.

Jahn G, Wendt J, Lotze M, Papenmeier F, Huff M (2012) Brain activation during spatial updating and attentive tracking of moving targets. Brain Cogn 78:105–113.

Jenkinson M, Bannister P, Brady M, Smith S (2002) Improved optimization for the robust and accurate linear registration and motion correction of brain images. Neuroimage 17:825–841.

Jovicich J, Peters RJ, Koch C, Braun J, Chang L, Ernst T (2001) Brain areas specific for attentional load in a motion-tracking task. J Cogn Neurosci 13:1048–1058.

Killebrew K, Mruczek R, Berryhill ME (2015) Intraparietal regions play a material general role in working memory: evidence supporting an internal attentional role. Neuropsychologia 73:12–24.

Kinsbourne M (1987) Mechanisms of unilateral neglect. In: *Advances in psychology: neurophysiology and neuropsychological aspects of spatial neglect* (Jeannerod M, ed), Vol. 45, pp. 69–86. Amsterdam: Elsevier Science.

Klein A, et al. (2017) Mindboggling morphometry of human brains. PLoS Comput Biol 13:e1005350.

Luck SJ, Hillyard SA, Mangun GR, Gazzaniga MS (1989) Independent hemispheric attentional systems mediate visual search in split-brain patients. Nature 342:543–545.

Luke SG (2017) Evaluating significance in linear mixed-effects models in R. Behav Res Methods 49:1494–1502.

Ma F, Guo J, Gobbini MI, Haxby JV (2023) A cortical surface template for human neuroscience. bioRxiv, 2023-03.

Maechler MR, Cavanagh P, Tse PU (2021) Attentional tracking takes place over perceived rather than veridical positions. Attent Percep Psychophys 83:1455–1462.

Merkel C, Hopf JM, Heinze HJ, Schoenfeld MA (2015) Neural correlates of multiple object tracking strategies. Neuroimage 118:63–73.

Merkel C, Hopf JM, Schoenfeld MA (2024) Location-and object-based representational mechanisms account for bilateral field advantage in multiple-object tracking. eNeuro 11:ENEURO.0519-23.2024.

Mesulam MM (1981) A cortical network for directed attention and unilateral neglect. Ann Neurol 10:309–325.

Mounts JR (2000) Evidence for suppressive mechanisms in attentional selection: feature singletons produce inhibitory surrounds. Attent Percept Psychophys 62:969–983.

Naert L, Bonato M, Fias W (2018) Asymmetric spatial processing under cognitive load. Front Psychol 9:348828.

Nummenmaa L, Oksama L, Glerean E, Hyönä J (2017) Cortical circuit for binding object identity and location during multiple-object tracking. Cereb Cortex 27:162–172.

Parton A, Malhotra P, Husain M (2004) Hemispatial neglect. J Neurol Neurosurg Psychiat 75:13–21.

Pelli DG (1997) The VideoToolbox software for visual psychophysics: transforming numbers into movies. Spat Vis 10:437–442.

Petersen SE, Posner MI (2012) The attention system of the human brain: 20 years after. Annu Rev Neurosci 35:73–89.

Posner MI, Petersen SE (1990) The attention system of the human brain. Annu Rev Neurosci 13:25–42.

Rosenke M, Van Hoof R, Van Den Hurk J, Grill-Spector K, Goebel R (2021) A probabilistic functional atlas of human occipito-temporal visual cortex. Cereb Cortex 31:603–619.

Saxe R, Brett M, Kanwisher N (2006) Divide and conquer: a defense of functional localizers. Neuroimage 30:1088–1096.

Scholl BJ (2009) What have we learned about attention from multiple-object tracking (and vice versa)?

Sheremata SL, Bettencourt KC, Somers DC (2010) Hemispheric asymmetry in visuotopic posterior parietal cortex emerges with visual short-term memory load. J Neurosci 30:12581–12588.

Shim WM, Alvarez GA, Vickery TJ, Jiang YV (2010) The number of attentional foci and their precision are dissociated in the posterior parietal cortex. Cereb cortex 20:1341–1349.

Störmer VS, Alvarez GA, Cavanagh P (2014) Within-hemifield competition in early visual areas limits the ability to track multiple objects with attention. J Neurosci 34:11526–11533.

Störmer VS, Winther GN, Li SC, Andersen SK (2013) Sustained multifocal attentional enhancement of stimulus processing in early visual areas predicts tracking performance. J Neurosci 33:5346–5351.

Strong RW, Alvarez GA (2020) Hemifield-specific control of spatial attention and working memory: evidence from hemifield crossover costs. J Vis 20:1–24.

Szczepanski SM, Kastner S (2013) Shifting attentional priorities: control of spatial attention through hemispheric competition. J Neurosci 33:5411–5421.

Tustison NJ, Avants BB, Cook PA, Zheng Y, Egan A, Yushkevich PA, Gee JC (2010) N4ITK: improved N3 bias correction. IEEE Trans Med Imag 29: 1310–1320.

Wang L, Mruczek RE, Arcaro MJ, Kastner S (2015) Probabilistic maps of visual topography in human cortex. Cereb Cortex 25:3911–3931.

Wilkinson GN, Rogers CE (1973) Symbolic description of factorial models for analysis of variance. J R Stat Soc Ser C 22:392–399.

Worsley KJ (2001) Statistical analysis of activation images. Funct MRI 14: 251–270.

Zhang Y, Brady M, Smith S (2001) Segmentation of brain MR images through a hidden Markov random field model and the expectation-maximization algorithm. IEEE Trans Med Imag 20:45–57.